# Pulse propagation effects in a cyclotron resonance maser amplifier

P. Aitken, B. W. J. McNeil, G. R. M. Robb, and A. D. R. Phelps
*Department of Physics and Applied Physics, University of Strathclyde, Glasgow G4 0NG, Scotland*
(Received 18 June 1998)

An analysis is presented of a cyclotron resonance maser amplifier operating with electron pulses. The electrons are resonant at two frequencies of the same waveguide mode. We consider both a single resonant frequency interaction and also a coupled two resonant frequency interaction. It is shown that, in general, the interaction with both resonant frequencies must be taken into account. The analysis includes propagation effects due to the difference between the axial velocity of the electrons and the group velocities of the radiation fields. Both linear and numerical solutions to the equations are given, and superradiant emission is demonstrated where the radiated power scales as the square of the electron pulse current. Two methods of low-frequency suppression are presented allowing the high-frequency emission to dominate. These results may have important consequences for the generation of short pulses of high-frequency, high-power microwave radiation. [S1063-651X(99)01001-6]

PACS number(s): 41.60.−m, 52.75.Ms, 84.40.Ik

## I. INTRODUCTION

Cyclotron resonance masers (CRMs) are important sources of coherent high-power microwave radiation. The radiation source of the CRM is a relativistic electron beam gyrating as it propagates along a uniform magnetic field, and the radiation emitted by the electrons is usually contained within a cylindrical waveguide structure. When the electrons interact with either their spontaneous radiation, or with an injected signal, a collective instability may bunch the electrons in the phase angle of the electron gyration, or the axial electron position, or both. The bunched electrons may then emit coherently. The collective instability may give an exponential growth of the radiation field until saturation, where free energy depletion [1] of the electron beam and/or a dephasing of the electron bunching occurs. In general, for a single waveguide mode, there exist two distinct resonant frequencies. In most circumstances it is the lower resonant frequency that has the larger growth rate and dominates the exchange of energy from the electrons to the radiation field. The electron source for the CRM is usually of a duration which is much greater than both the resonant radiation period and the time of flight of a typical electron through the interaction region [2–5]. Considerable mathematical analysis has therefore been carried out, assuming interaction at a single resonant frequency only, and using the ''steady state'' approximation, which assumes a uniform current electron beam of infinite duration [1,5–15].

More recently, an analysis of the steady state amplifier interaction allowing both the lower and higher resonant frequency fields to evolve has shown that it is possible to suppress the evolution of the lower frequency instability [16], possibly allowing the CRM to operate at the higher frequency only. When the steady state approximation is not valid, the relative propagation of the electron pulse with respect to the radiation emitted becomes important, and may give rise to new regimes of operation. With the advances in accelerator technology [17–20], pulse dominated CRM operation is now possible with ultrashort pulse durations of the order of the radiation period being feasible [21]. The pulsed ''superradiant'' regime, where the radiation power emitted scales as the square of the electron current, is of particular interest [22,23], and has many conceptual similarities with superradiant behavior in free electron lasers [24–26]. Superradiant emission offers a possible method of generating very short high-power pulses of microwave radiation.

In this paper we present results arising from a detailed analytical and numerical investigation of CRMs operating in this pulsed amplifier regime. Clearly the fact that pulses of radiation are generated increases the frequency bandwidth when compared with that of the steady state regime. The analysis is first performed for a single resonant frequency interaction, and then for simultaneous interaction at the lower and higher resonant frequencies. In both cases superradiant emission from the electron pulses is demonstrated, and it is shown that, in general, the coupled interaction with both resonant frequencies must be taken into account. In addition, two methods of suppressing the lower resonant frequency are presented. These results may have important consequences for the generation of short pulses of high-frequency, high-power microwave radiation.

The resonant frequencies of the CRM interaction may be determined by the intersection of the waveguide and beam modes as defined by

$$\omega^2 = \omega_c^2 + k_\parallel^2 c^2, \tag{1}$$

$$\omega = \omega_H + k_\parallel v_\parallel, \tag{2}$$

respectively, where $\omega_c$ is the waveguide cutoff frequency, $k_\parallel$ is the axial component of the radiation wave vector, $\omega_H$ is the relativistic cyclotron frequency and $v_\parallel$ is the axial velocity of the electrons. A typical dispersion diagram in Fig. 1(a) shows the intersections at the two resonant frequencies. The radiation at the higher resonant frequency has an axial group velocity ($v_g = \partial\omega/\partial k_\parallel$) greater than that of the lower resonant frequency, and so these resonant modes are defined as being the ''fast'' and ''slow'' resonant modes, respectively.

 

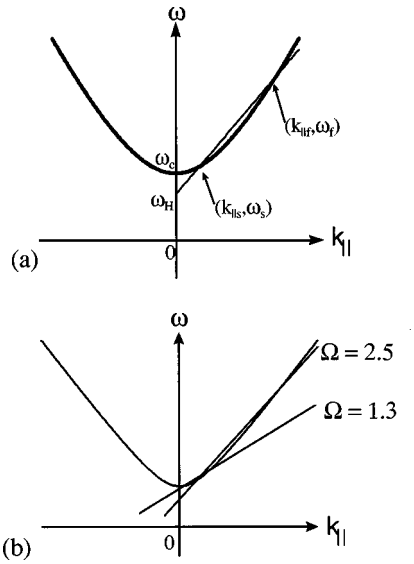


FIG. 1. (a) Dispersion diagram showing the intersection of electron beam and waveguide modes. (b) Dispersion diagram illustrating the different operating regimes for two values of the device parameter $\Omega$ for $\epsilon=2$ ($\Omega_{\max}=4$).

Solving Eqs. (1) and (2), we obtain solutions for the fast and slow mode resonant frequencies and their corresponding axial wave vectors:

$$\omega_{f,s}=\omega_H\frac{1\pm\beta_\|\sqrt{1-X}}{1-\beta_\|^2}, \tag{3}$$

$$k_{\|f,s}=\frac{\omega_H}{c}\frac{\beta_\|\pm\sqrt{1-X}}{1-\beta_\|^2}, \tag{4}$$

where the ''waveguide parameter'' $X=\omega_c^2/(\omega_H^2\gamma_\|^2)$, $\beta_\|=v_\|/c$, $\gamma_\|=(1-\beta_\|^2)^{-1/2}$ and subscripts $f$ and $s$ indicate the fast and slow modes, respectively. In this paper we consider the case where both the fast and slow modes propagate in the forward direction only. This limits the range of the waveguide parameter, $X$, to

$$1/\gamma_\|^2<X<1. \tag{5}$$

Note that the upper limit on $X$ implies that the relativistic cyclotron frequency, in the drift frame of the electrons, must be greater than the waveguide cutoff frequency.

The ''device parameter'' $\Omega$, is defined as in Ref. [16] to be

$$\Omega=\frac{2}{X}-1=\frac{1}{\omega_c^2}(\omega_f\omega_s-k_{\|f}k_{\|s}c^2), \tag{6}$$

and is constrained to lie within the limits

$$1<\Omega<\Omega_{\max},$$

where $\Omega_{\max}=(1+\epsilon^6)/(2\epsilon^3)$ and $\epsilon^3=k_{\|f}/k_{\|s}$. The upper limit on $\Omega$ is for the limit $\omega_c\to 0$. If $\Omega$ lies toward the minimum of the interval, then the interaction is of the gyrotron type; conversely, if $\Omega$ lies toward the maximum of the interval then the interaction is of the cyclotron autoresonance maser type. Figure 1(b) shows the different regimes of operation as $\Omega$ increases from $\Omega\approx 1$ to $\Omega\approx\Omega_{\max}$. For finite values of $\epsilon$ the upper limit $\Omega_{\max}$ places a more restrictive lower limit on the value of $X$ than that of Eq. (5), giving a range of allowable values $4\epsilon^3/(\epsilon^3+1)^2<X<1$.

The CRM interaction may be considered at only one of the resonant modes, either fast or slow. We call this the single mode model, and it has previously been the subject of substantial interest [1,5–15]. These works have been conducted in the steady state regime, which neglects propagation effects due to the difference between the group velocities of the radiation and the average axial velocity of the electrons. In one of those works [13], the equations describing the CRM interaction were written in a scaled form in terms of two physically meaningful scaling parameters. The first is the fundamental CRM parameter, $\rho$, analogous to the Pierce parameter of traveling wave tube (TWT) theory [27], and determines the growth rate of the electron/radiation instability. The second is the depletion parameter $\mu$, which describes the effects of free energy depletion of the electron beam [1]. The depletion parameter is a measure of the ability of the interaction to convert the energy associated with the cyclotron motion of the electrons into radiation. For small values of the depletion parameter, only a small fraction of this energy is available. The fundamental CRM parameter $\rho$, and the depletion parameter $\mu$, are related via the relation

$$\mu=\frac{\rho}{\nu}, \tag{7}$$

where $\nu$ is the free energy parameter, and is a measure of the transverse energy content of the electron beam relative to the axial energy [13,16]. Linear theory shows that there is a threshold value of the depletion parameter, $\mu_{\rm th}$, above which no exponential growth of the radiation field is possible. Any two of the three parameters $\rho$, $\mu$, and $\nu$, defined in Sec. II may be used in the scaling of the equations describing the interaction. Here, as in our previous publications, we have chosen the fundamental CRM parameter and the depletion parameter as our primary scaling parameters.

In a two mode interaction, however, we are free to choose between the $\rho$ and $\mu$ parameters of the fast or the slow modes, which we designate with subscripts $f$ and $s$, respectively. In this paper the fast mode scaling is chosen, conversion to slow mode scaling being straightforward via the relations

$$\rho_f=\epsilon^2\rho_s, \quad \mu_f=\mu_s/\epsilon. \tag{8}$$

Note that $\rho_f$ is bounded within the interval

$$0<\rho_f<2\mu_f\epsilon^3/(\epsilon^3+1), \tag{9}$$

the upper limit resulting from the restriction $v_\|<c$. This upper limit on the value of $\rho_f$ limits the growth rate of the radiation and also the efficiency of the device [16]. Summarizing, in total four parameters are required to describe the CRM coupled interaction between the fast and slow modes: the axial wave vector ratio $\epsilon$; the device parameter $\Omega$; the CRM parameter for the fast mode, $\rho_f$; and the depletion parameter of the fast mode, $\mu_f$.

A linear and numerical analysis of the coupled two mode interaction has been conducted in the steady state regime where propagation effects are neglected [16]. Here the interaction of the slow mode has a larger growth rate, except for a small region of parameter space where linear theory and numerical simulation predict no exponential growth of the slow mode for a range of the depletion parameter $\mu_f$. This range corresponds to that where, due to the scaling of Eq. (8), the value of the depletion parameter of the fast mode is below threshold ($\mu_f<\mu_{\rm th}$), but that for the slow mode is above threshold ($\mu_s>\mu_{\rm th}$):

$$\frac{1}{\epsilon}\left[\left(\frac{27}{32}\right)^{1/3}+\frac{\rho_f}{2\epsilon^2}\right]<\mu_f<\left(\frac{27}{32}\right)^{1/3}+\frac{\rho_f}{2}. \tag{10}$$

Hence choice of $\mu_f$ from within this region allows for a ''$\mu$ suppression'' of the lower frequency slow mode.

In the steady state regime the radiation intensity scales as $n_e^{4/3}$, where $n_e$ is the electron density; however, when propagation effects are included in the model, there is another regime of operation known as the superradiant regime [23], where the radiation intensity scales as $n_e^2$. The purpose of this paper is to investigate the CRM interaction for electron pulses, including propagation effects, for both the single frequency and two frequency regimes [23,28]. Of fundamental importance when discussing electron pulses is the cooperation length. This length is the minimum distance within the electron pulse between which electrons may interact cooperatively, and may be defined as the relative slippage distance between the radiation envelope and the electron pulse in one gain length. An electron pulse is defined to be long or short with respect to a length proportional to the cooperation length. However, both the slippage distance and the gain length are different for the two frequencies of the fast and slow modes, and so the cooperation length is different for each frequency. Due to this frequency dependent cooperation length it is possible for the same electron pulse to be long with respect to the higher frequency cooperation length and short with respect to the lower frequency cooperation length. Typically short pulses give rise to a weak superradiant interaction in which the intensity of the radiation emitted is less than that from long pulses where strong superradiance and steady state effects dominate. By choosing a scaled electron pulse length that is long with respect to the high-frequency fast mode, and short with respect to the low-frequency slow mode, suppression of the latter is possible. We call such suppression of the slow mode ''pulse suppression.''

A linear analysis is presented and a comparison made with numerical solutions of both linear and nonlinear interactions. The two methods of slow mode suppression, $\mu$ suppression and pulse suppression, are presented using both short and long electron pulses.

## II. SCALED EQUATIONS

The set of scaled equations which describe the pulse evolution in a CRM are the partial differential form of those derived in the steady state [16]. We start from the coupled Maxwell-Lorentz equations describing the radiation and electron beam evolution as described in Ref. [13]. A thin annular electron beam propagating in the positive $\hat{\mathbf{z}}$ direction along a cylindrical waveguide containing ''cold'' $\mathrm{TE}_{m,n}$ waveguide modes is assumed. The waveguide is coaxial with a static magnetic field $\mathbf{B}=B_0\hat{\mathbf{z}}$. These modes are defined by the cylindrical components of the electric fields:

$$E_{f,s}^{(r)}=-\frac{m}{2r}F_{f,s}(z,t)D_{\rm TE}J_m(k_\perp r)e^{i\Psi_{f,s}}+\text{c.c.},$$

$$E_{f,s}^{(\theta)}=\frac{ik_\perp}{2}F_{f,s}(z,t)D_{\rm TE}J_m'(k_\perp r)e^{i\Psi_{f,s}}+\text{c.c.},$$

$$E_{f,s}^{(z)}=0,$$

where

$$\Psi_{f,s}=\omega_{f,s}t-m\theta-k_{\parallel f,s}z,$$

$$D_{\rm TE}=\frac{1}{J_m(\chi_{mn}')\sqrt{\pi(\chi_{mn}'^2-m^2)}},$$

$k_\perp$ is the transverse component of the radiation wave vector, $\chi_{mn}'$ is the $n$th root of $J_m'(k_\perp R_w)=0$ and $R_w$ is the waveguide radius. The field is assumed to obey the slowly varying envelope approximation (SVEA) so that $F_{f,s}(z,t)=|F_{f,s}(z,t)|e^{i\xi_{f,s}(z,t)}$ is a slowly varying complex envelope function determining the $z$ and $t$ dependence of the amplitude and phase of the radiation field.

The product of the transverse component of the radiation wave vector, and the Larmor radius of the gyrating electrons is assumed small, i.e., $k_\perp r_L<1$. This is an experimentally desirable approximation which maximizes coupling with the radiation mode when the electron beam annulus is coincident with the maximum of the transverse mode electric field. Further, it is assumed there are no space charge effects and that the electron beam phase evolution is slow with respect to the cyclotron period. The latter allows the Maxwell-Lorentz equations to be averaged over a cyclotron period. The effect of beating between the two radiation frequencies is also neglected by averaging the wave equations over a beat period, which under the SVEA is valid for $\omega_f\gtrsim 2\omega_s$. This is in contrast to the work of [21,22], where ''group synchronism'' between the beam mode and the waveguide mode is assumed ($v_{g_f}\approx v_{g_s}\approx v_\parallel$). This minimizes the effects of the relative slippage between the fast and slow resonant modes, and puts the interaction into a regime where the effects of the beating between these modes and waveguide dispersion cannot be neglected. The work presented here is therefore not applicable to the experimental results of Ref. [21]. With these approximations the coupled Maxwell-Lorentz equations reduce to the following forms:

$$\frac{d\phi_{f_j}}{d\bar{z}_f}=\bar{p}_{f_j}-\frac{i\mu_f}{\bar{u}_{\perp_j}\bar{u}_{\parallel_j}}(\bar{A}_f e^{i\phi_{f_j}}+\epsilon^2\bar{A}_s e^{i\phi_{s_j}}-\text{c.c.}), \tag{11}$$

$$\frac{d\bar{z}_{1_{f_j}}}{d\bar{z}_f}=\frac{\rho_f}{\Omega-1}(\epsilon\bar{p}_{s_j}-\bar{p}_{f_j}), \tag{12}$$

$$\frac{d\bar{p}_{f_j}}{d\bar{z}_f}=\frac{\bar{u}_{\perp_j}}{\bar{u}_{\parallel_j}^2}\left[(\rho_f\bar{p}_{f_j}-1)\bar{A}_f e^{i\phi_{f_j}}+\left(\frac{\rho_f}{\epsilon}\bar{p}_{f_j}-\epsilon^2\Omega\right)\bar{A}_s e^{i\phi_{s_j}}+\text{c.c.}\right], \tag{13}$$

$$\frac{d\bar{p}_{s_j}}{d\bar{z}_f}=\frac{\bar{u}_{\perp_j}}{\bar{u}_{\parallel_j}^2}\left[\left(\rho_f\bar{p}_{s_j}-\frac{\Omega}{\epsilon}\right)\bar{A}_f e^{i\phi_{f_j}}+\left(\frac{\rho_f}{\epsilon}\bar{p}_{s_j}-\epsilon\right)\bar{A}_s e^{i\phi_{s_j}}+\text{c.c}.\right], \tag{14}$$

$$\frac{d\bar{u}_{\perp_j}}{d\bar{z}_f}=-\frac{\mu_f}{\bar{u}_{\parallel_j}}(\bar{A}_f e^{i\phi_{f_j}}+\epsilon^2\bar{A}_s e^{i\phi_{s_j}}+\text{c.c.}), \tag{15}$$

$$\frac{d\bar{u}_{\parallel_j}}{d\bar{z}_f}=-\frac{\bar{u}_{\perp_j}\rho_f}{\bar{u}_{\parallel_j}}\left(\bar{A}_f e^{i\phi_{f_j}}+\frac{1}{\epsilon}\bar{A}_s e^{i\phi_{s_j}}+\text{c.c.}\right), \tag{16}$$

$$\left(\frac{\partial}{\partial\bar{z}_f}+\frac{\partial}{\partial\bar{z}_{1_f}}\right)\bar{A}_f(\bar{z}_f,\bar{z}_{1_f})=\bar{b}_f, \tag{17}$$

$$\left(\frac{\partial}{\partial\bar{z}_f}-\epsilon^3\frac{\partial}{\partial\bar{z}_{1_f}}\right)\bar{A}_s(\bar{z}_f,\bar{z}_{1_f})=\epsilon\bar{b}_s, \tag{18}$$

where

$$j=1,\ldots,N,\quad \bar{z}_f=\frac{z}{l_{g_f}},\quad \bar{t}_f=\frac{v_{g_f}t}{l_{g_f}},\quad \bar{z}_{1_f}=\frac{\bar{z}_f-\beta_f\bar{t}_f}{1-\beta_f},$$

$$\phi_{f,s}=\omega_{f,s}t-k_{\parallel_{f,s}}z+\tan^{-1}\left(\frac{u_y}{u_x}\right)-(m-1)\theta_0-\frac{\pi}{2},$$

$$\bar{u}_{\perp_j}=\frac{u_{\perp_j}}{u_{\perp 0}},\quad \bar{u}_{\parallel_j}=\frac{u_{\parallel_j}}{u_{\parallel 0}},\quad u_{\perp_j}=\gamma v_\perp,\quad u_{\parallel_j}=\gamma v_\parallel,$$

$$\bar{A}_{f,s}=\frac{ieu_{\perp 0}k_{\parallel f,s}^2 D_{TE}J_{m-1}(k_\perp R_0)}{4m_e u_{\parallel 0}^2 k_\perp\omega_{f,s}\rho_{f,s}^2}F_{f,s},$$

$$\bar{p}_{f,s}=\frac{k_{\parallel f,s}}{k_\perp^2}\frac{1}{\rho_{f,s}}p_{f,s},\quad p_{f,s}=\frac{1}{v_\parallel}(\omega_{f,s}-\omega_H)-k_{\parallel f,s},$$

$$k_{H0}=\frac{\gamma\omega_H}{u_{\parallel 0}},$$

$$\rho_{f,s}=\left(\frac{e}{8\epsilon_0 m_e c^2}\frac{k_{\parallel f,s}^2}{k_\perp^2}\frac{u_{\perp 0}^2}{u_{\parallel 0}^3}ID_{\text{TE}}^2J_{m-1}^2(k_\perp R_0)\right)^{1/3},$$

$$\nu_{f,s}=\frac{k_{\parallel f,s}}{k_{H0}}\frac{u_{\perp 0}^2}{u_{\parallel 0}^2},\quad \mu_{f,s}=\frac{\rho_{f,s}}{\nu_{f,s}},\quad l_{g_f}=\frac{k_f}{k_\perp^2\rho_f},$$

$$\bar{b}_{f,s}=\frac{1}{N_{b_0}}\sum_{j=1}^{N_b}\chi_j\frac{\bar{u}_{\perp_j}}{\bar{u}_{\parallel_j}}e^{-i\phi_{f,s_j}}.$$

$j$ is the electron index number, $N$ is the total number of (macro) electrons; $N_b$ is the number of (macro)electrons in the beat period centered at position $\bar{z}_{1_f}$; $\chi_j$ are the macroelectron charge weightings normalized with respect to the value evaluated at the peak current $I$, so that $0<\chi_j\leqslant 1$; subscripts $\perp$ and $\parallel$ represent vector components perpendicular and parallel to the waveguide axis; $r_L$ is the Larmor radius of a gyrating electron; $\gamma$ is the electron relativistic factor; $(R_0,\theta_0)$ are the polar coordinates with respect to the waveguide axis of the electron guiding centers; $(v_\perp,v_\parallel)$ are the electron velocity components; $\beta_{f,s}=v_\parallel/v_{g_{f,s}}$ is the ratio of the axial electron to group velocities; $l_{g_f}$ is the gain length for the fast mode; and subscripts 0 indicate initial values on entering the interaction region at $\bar{z}_f=0$. The geometry of the electron beamlet illustrating the geometric variables is shown in Fig. 2. In all of the following work we assume an electron pulse with a rectangular current distribution, so that $\chi_j=1\forall j$. We also assume that there is no cavity feedback, so that the system acts as a single pass amplifier.

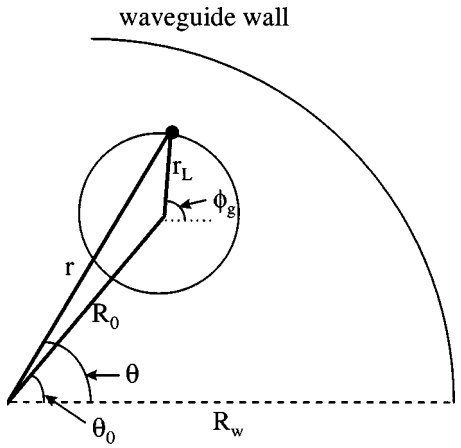


FIG. 2. A schematic of an electron beamlet showing the relevant geometry.

With the exception of the scaling and the consideration of two radiation frequencies, the derivation of Eqs. (11)–(18) follows a similar course to that of previous works [5–13]. Use has been made of Graf's theorem for Bessel functions in averaging the equations over a cyclotron period. An electron is said to be resonant with a radiation field when $\delta_{f,s}=\bar{p}_{f,s}(\bar{z}_f=0)=0$. Evolution of a resonant, or nearly resonant, electron beam allows a ''slow'' exchange of energy between the beam and the radiation. In deriving Eqs. (11)–(18) the independent variables have been scaled with respect to the fast mode parameters. Scaling with respect to the slow mode is possible via the relations

$$\bar{z}_s=\epsilon\bar{z}_f\quad \bar{z}_{1_s}=\frac{1}{\epsilon^2}(\bar{l}_{e_f}-\bar{z}_{1_f}), \tag{19}$$

where $\bar{l}_{e_f}$ is the length of the electron pulse $l_e$ scaled in units of $\bar{z}_{1_f}$.

We define the relative propagation distance of the radiation envelope with respect to the electron pulse to be the slippage distance. Furthermore, we define a cooperation

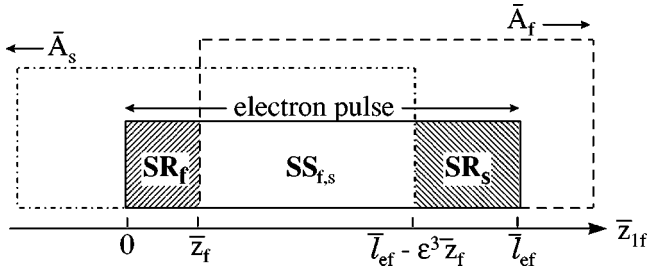


FIG. 3. Schematic representation of the electron pulse and radiation field envelopes illustrating the slippage regions (SR) (hatched) and the steady state (SS) region of the electron pulse. Superradiant emission of the fast and slow modes is confined to regions ($SR_f$) and ($SR_s$), respectively.

length to be the slippage distance in one gain length. It can be shown that the cooperation lengths for both fast and slow modes are given by

$$l_{c_{f,s}} = \frac{1-\beta_{f,s}}{\beta_{f,s}} l_{g_{f,s}}. \tag{20}$$

With these definitions the scaled length of the electron pulse may be written as

$$\bar{l}_{e_{f,s}} = \frac{l_e}{\beta_{f,s} l_{c_{f,s}}}. \tag{21}$$

Historically this formalism was developed for free electron laser (FEL) theory where the $\beta$ in the denominator of (21) is approximately one [24–26]. The electron pulse was then defined as being either long or short with respect to the cooperation length. Here, however, $\beta_{f,s}$ need not be approximately 1, and we redefine the pulse as being long or short with respect to $\beta_{f,s} l_{c_{f,s}}$. In this way we consider pulses to be short for $\bar{l}_{e_{f,s}} \lesssim 1$ and long for $\bar{l}_{e_{f,s}} \gg 1$. This scaled length is an important measure of the total gain experienced by the radiation as it propagates through the electron pulse. Using the scaling of Eq. (19), it can be shown that $\bar{l}_{e_f} = \epsilon^2 \bar{l}_{e_s}$ and as $\epsilon > 1$, the scaled pulse length of the fast mode is greater than that of the slow and may result in ''pulse suppression'' of the latter.

## III. LINEAR ANALYSIS

A linear analysis of Eqs. (11)–(18) is performed for the case of zero spread in electron energy and transverse momenta, using the method of ''collective variables'' as described in Ref. [29]. This shows that in the linear regime the fast and slow modes are decoupled and evolve independently, as was the case for the steady state [16]. Following the analysis of Refs. [23,25], it is found that for both fast and slow modes, in addition to the usual steady state solutions, there exist solutions which correspond to superradiant processes, where the intensity of the electromagnetic fields scales as the square of the number of emitters. Such superradiant emission is confined to the slippage regions of the electron pulse as defined by the shaded regions of Fig. 3.

For convenience the following variables are introduced:

$$A'_f = \bar{A}_f e^{i\delta_f \bar{z}}, \quad A'_s = \bar{A}_s e^{i\epsilon\delta_s \bar{z}}, \quad \phi'_f = \phi_f - \delta_f \bar{z},$$

$$\phi'_s = \phi_s - \epsilon\delta_s \bar{z}, \quad p'_f = \bar{p}_f - \delta_f, \quad p'_s = \bar{p}_s - \delta_s,$$

and the equations are linearized about their equilibrium values

$$A'_{f,s} = 0, \quad \langle e^{-i\phi'_{f,s}} \rangle = 0,$$

$$\bar{u}_{\perp_j} = 1, \quad \bar{u}_{\parallel_j} = 1, \quad p'_{f,s_j} = 0 \quad \forall j,$$

with collective variables defined by

$$b_f = -i\langle \phi'_{f_1} e^{-i\phi'_{f_0}} \rangle, \quad b_s = -i\langle \phi'_{s_1} e^{-i\phi'_{s_0}} \rangle,$$

$$P_f = \langle p'_{f_1} e^{-i\phi'_{f_0}} \rangle, \quad P_s = \langle p'_{s_1} e^{-i\phi'_{s_0}} \rangle,$$

$$U_{\perp f} = \langle \bar{u}_{\perp_1} e^{-i\phi'_{f_0}} \rangle, \quad U_{\perp s} = \langle \bar{u}_{\perp_1} e^{-i\phi'_{s_0}} \rangle,$$

$$U_{\parallel f} = \langle \bar{u}_{\parallel_1} e^{-i\phi'_{f_0}} \rangle, \quad U_{\parallel s} = \langle \bar{u}_{\parallel_1} e^{-i\phi'_{s_0}} \rangle.$$

all subscripts 1 referring to small changes from the equilibrium values subscripted 0 at $\bar{z}_f = 0$.

Using the collective variable description and the method of Laplace transforms, it is possible to reduce systems (11)–(18) to two uncoupled first order linear ordinary differential equations in the complex Laplace transformed field amplitudes $\tilde{A}_{f,s}(\lambda_{f,s}, \bar{t}'_{f,s})$:

$$\frac{d\tilde{A}(\lambda, \bar{t}')}{d\bar{t}'} + \frac{i\Delta(\lambda)}{(1-\beta)\lambda^2} \tilde{A}(\lambda, \bar{t}') = \frac{1}{(1-\beta)} \left( A'_0(\bar{t}') - \frac{i b_0(\bar{t}')}{\lambda} \right) \tag{22}$$

where

$$\tilde{A}(\lambda, \bar{t}') = \int_0^\infty A'(\bar{z}', \bar{t}') e^{i\lambda \bar{z}'} d\bar{z}', \tag{23}$$

$$\Delta(\lambda) = \lambda^3 - \delta\lambda^2 + (\rho - 2\mu)\lambda + (1 - \rho\delta), \tag{24}$$

with boundary conditions

$$A'(\bar{z}' = 0, \bar{t}') = A'_0(\bar{t}'), \quad b(\bar{z}' = 0, \bar{t}') = b_0(\bar{t}'). \tag{25}$$

The variables $\bar{z}' = \bar{z}$, $\bar{t}' = \bar{z} - \beta\bar{t}$, and the $f$ and $s$ subscripts have been omitted as the form of Eq. (22) is identical for both modes. Here we consider a constant initial field and no initial bunching, consistent with a single pass amplifier configuration

$$A'(\bar{z}', \bar{t}' = 0) = A'_0 e^{i\delta\bar{z}'}, \quad b(\bar{z}', \bar{t}' = 0) = 0.$$

Taking the inverse Laplace transform of the solution to Eq. (22) results in a solution for $A'(\bar{z}, \bar{t})$ which can be expressed as the sum of two terms:

$$A'(\bar{z}, \bar{t}) = A'_{SS}(\bar{z}) + A'_2(\bar{z}, \bar{t}). \tag{26}$$

The first term depends only upon $\bar{z}$, and is determined by the residues of the three simple poles $\lambda_{1,2,3}$ which are the roots of the dispersion relation $\Delta(\lambda)=0$. For $\bar{z}\gtrsim 1$ the form of $\bar{A}_{SS}$ is therefore just that of the steady state [16], which for $\delta,\rho,\mu\ll 1$ gives the scaled field intensity

$$\bar{I}_{SS}=|\bar{A}_{SS}(z)|^2\approx\frac{|\bar{A}_0|^2}{9}\exp\left(\frac{\sqrt{3}z}{l_g}\right). \tag{27}$$

The gain length $l_g$ is therefore the distance over which the field intensity increases by factor of $e^{\sqrt{3}}$ in this linear regime. When free energy depletion effects are included in the analysis, it is found that there is a threshold value of the depletion parameter $\mu_{th}=(\frac{27}{32})^{1/3}+\rho/2$ above which no exponential growth of the field occurs.

The second term in Eq. (26) is both space $(\bar{z})$, and time $(\bar{t})$, dependent, and so may describe a pulse structure. Contributions to this term come from the residues of the three simple poles $\lambda_{1,2,3}$ and from the residue of an essential singularity at $\lambda=0$. Defining a new variable

$$\bar{z}_2=\frac{\beta}{1-\beta}(\bar{t}-\bar{z})$$

so that $\bar{z}=\bar{z}_1+\bar{z}_2$, the second term in Eq. (26) can be written as

$$A_2'(\bar{z}_1,\bar{z}_2)=-\frac{iA_0'}{2\pi}e^{i\delta\bar{z}_1}\int_{-\infty-i\sigma}^{\infty-i\sigma}\frac{e^{i\lambda\bar{z}_2}}{\bar{\Delta}(\lambda)}\left(\frac{(c_1\lambda+c_0)}{\lambda-\delta}\right)\times\exp\left[-i\left(\frac{c_1}{\lambda}+\frac{c_0}{\lambda^2}\right)\bar{z}_1\right]d\lambda. \tag{28}$$

where $c_0=1-\rho\delta$ and $c_1=\rho-2\mu$. When $\bar{z}_2<0$, the contribution from $A_2'(\bar{z}_1,\bar{z}_2)$ is zero, and the resultant field amplitude is just that due to the steady state. Conversely, if $\bar{z}_2>0$, then $A_2'(\bar{z}_1,\bar{z}_2)=-A_{SS}'(\bar{z})+A_{SR}'(\bar{z}_1,\bar{z}_2)$, and the resultant field will be $A'(\bar{z}_1,\bar{z}_2)=A_{SR}'(\bar{z}_1,\bar{z}_2)$, where $A_{SR}'(\bar{z}_1,\bar{z}_2)$ arises from the essential singularity at $\lambda=0$ alone. When $\bar{z}_1>0$ and $\bar{z}_2>0$, evolution is due to a different process from that which produces steady state evolution and gives rise to superradiance. From the definitions of $\bar{z}_1$ and $\bar{z}_2$, the regions where superradiance may occur are the slippage regions shown in Fig. 3. The slippage region for the fast mode is at the electron pulse tail defined by the region $0<\bar{z}_{1_f}<\bar{z}_f$, and for the slow mode at the front of the pulse defined by the region $\bar{l}_{e_f}-\epsilon^3\bar{z}_f<\bar{z}_{1_f}<\bar{l}_{e_f}$. Between the two slippage regions is an area where steady state emission occurs until $\bar{z}_f>\bar{l}_{e_f}/(1+\epsilon^3)$ when the two slippage regions overlap. It was previously shown in Ref. [16] that for long electron pulses $(\bar{l}_e\gg 1)$, and for the steady state region within the pulse, the slow mode growth can be suppressed using the $\mu$-suppression condition of Eq. (10), and the fast mode dominates the interaction.

A threshold condition for exponential growth of the radiation fields, analogous to that of the steady state, applies to the slippage regions of both the fast and slow modes and occurs within the regions of the pulse defined by ($f$ and $s$ subscripts assumed)

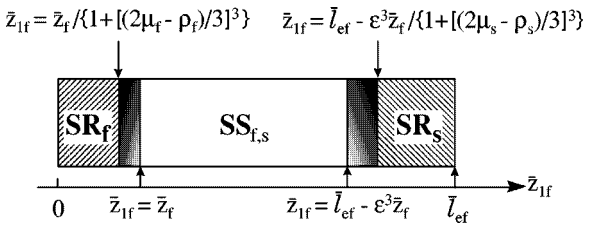


FIG. 4. Region of no exponential growth (shaded) within the slippage regions (hatched) of the fast and slow modes.

$$\bar{z}<\bar{z}_1<\frac{\bar{z}}{1+\left(\frac{2\mu-\rho}{3}\right)^3}. \tag{29}$$

These regions of the pulse are shown, using fast-scaled variables, in Fig. 4. It is seen, recalling the upper limit of $\rho$ from Eq. (9), that this region disappears in the FEL limit $\mu\to 0$.

The rate at which the boundary of the exponential instability moves within the slippage region is given by

$$\frac{d\bar{z}_1}{d\bar{z}}=\frac{1}{1+\left(\frac{2\mu-\rho}{3}\right)^3}<1,$$

whereas that for the boundary between the slippage region and the steady state is

$$\frac{d\bar{z}_1}{d\bar{z}}=1.$$

Hence the shaded regions of Fig. 4 expand as the interaction proceeds with increasing $\bar{z}$. In the high gain regime $(\bar{z}>1)$ the shaded nonexponential regions will lie out with the electron pulse, and so do not affect the interaction, for scaled pulse lengths

$$\bar{l}_e<\frac{1}{1+\left(\frac{2\mu-\rho}{3}\right)^3},$$

and it would be expected that there will be little suppression of the exponential instability. For long pulses, however, where

$$\bar{l}_e\gg\frac{1}{1+\left(\frac{2\mu-\rho}{3}\right)^3},$$

and for larger values of $\mu$, the effects of the nonexponential region would be expected to be more pronounced. It will be seen from computational simulations into the non-linear regime that this is the case.

In the limit of $\mu\ll 1$ an asymptotic approximation for the solution to $A_{SR}'(\bar{z}_1,\bar{z}_2)$ can be obtained using the method of

stationary phase as described in Ref. [25]. The linear solution for the complex field can then be approximated in the limit of large $x$ by

$$\overline{A}_{\mathrm{SR}} \approx \frac{\overline{A}_0}{2^{2/3}\sqrt{3\pi}x^{1/2}Q(\overline{z}_1,\overline{z}_2)} \times \exp\left(\frac{3}{2}(\sqrt{3}+i)\frac{x}{2^{2/3}} + i\delta\overline{z}_1 - \frac{i\pi}{12}\right), \tag{30}$$

where

$$x=(\overline{z}_1\overline{z}_2^2)^{1/3},$$

$$\overline{z}=\overline{z}_1+\overline{z}_2,$$

$$Q(\overline{z}_1,\overline{z}_2)=1+\delta\left(\frac{2\overline{z}_1}{\overline{z}_2}\right)^{2/3}\exp\left(\frac{i\pi}{3}\right)-\frac{2\overline{z}_1}{\overline{z}_2}.$$

Using Eq. (30), the ratio of the scaled intensities of the radiation for the fast and slow modes as they exit the electron pulse of length $\overline{l}_{e_f}$ (at the leading edge of the electron pulse for the higher frequency and at the trailing edge for the lower) is

$$\frac{\overline{I}_f(\overline{z}_{1_f}=\overline{l}_{e_f},\overline{z}_f)}{\overline{I}_s(\overline{z}_{1_f}=0,\overline{z}_f)} = \left(\frac{\overline{z}_f-\overline{l}_{e_f}}{\epsilon^3\overline{z}_f-\overline{l}_{e_f}}\right)^{4/3}\left(\frac{\epsilon^3\overline{z}_f-3\overline{l}_{e_f}}{\epsilon(\overline{z}_f-3\overline{l}_{e_f})}\right)^2 \times \exp\left[\frac{3\sqrt{3}}{2^{2/3}}\overline{l}_{e_f}^{1/3}\left((\overline{z}_f-\overline{l}_{e_f})^{2/3} - \frac{1}{\epsilon^2}(\epsilon^3\overline{z}_f-\overline{l}_{e_f})^{2/3}\right)\right], \tag{31}$$

where use has been made of the relation

$$\overline{z}_{2_s}=\epsilon\overline{z}_f-\frac{1}{\epsilon^2}(\overline{l}_{e_f}-\overline{z}_{1_f}), \tag{32}$$

and equal initial scaled intensities for the fast and slow modes with no initial bunching have been assumed ($\overline{A}_{f_0}=\overline{A}_{s_0}, b_{f_0}=b_{s_0}=0$). Note from the scaling that the ratio of real, unscaled, intensities is given by

$$\frac{I_f}{I_s}=\frac{\epsilon^3\Omega-1}{\epsilon(\epsilon^3-\Omega)}\frac{\overline{I}_f}{\overline{I}_s}. \tag{33}$$

In Fig. 5 a plot of ratio (31) as a function of scaled electron pulse length $\overline{l}_{e_f}$ is shown. It is seen that as the electron pulse length increases so the ratio decreases. This shows that for sufficiently short electron pulses, emission at the higher frequency fast mode can be substantially greater than in the steady state where, without $\mu$ suppression, the slow mode dominates. We call this pulse suppression of the slow mode. Although the slow mode has a higher growth rate than the fast mode, its scaled pulse length $\overline{l}_{e_s}$ is shorter. Thus the slow mode may experience less gain than the fast mode. It will be shown that this mechanism provides a method for suppressing the growth of the slow mode in short electron pulses, allowing the higher frequency fast mode to dominate.

## IV. NUMERICAL MODEL

In order to describe the evolution of the coupled radiation fields and electrons numerically, the method of finite elements is applied [30]. This method assigns radiation field values to a set of nodal grid points, allowing a pulse structure to be described. The value of the fields at each node evolves due to the interaction with the electrons. Between nodes, interpolation is used to calculate the fields so that they vary continuously throughout the pulse. Furthermore, the driving terms of the wave equations are also assigned to nodal grid points.

In the case considered here, where there are two copropagating radiation fields, two sets of nodal grid points are required, one set for each field. The scaled radiation fields and driving terms at the $n$th node are defined as $\overline{A}_{f,s_n}(\overline{z}_f)$ and $\overline{b}_{f,s_n}(\overline{z}_f)$, respectively.

For positions intermediate to these nodes the field is reconstructed by interpolation from the nodal values as shown in Fig. 6(a). For the case illustrated a linear interpolation function is shown. For higher order interpolation extra nodes internal to the elements will be required [30]. Both the scaled fields and driving terms may be approximated by a sum over the elements of the interpolated nodal values,

$$\overline{A}_{f,s}(\overline{z}_f,\overline{z}_{1_f}) \approx \sum_{e=1}^{N_e} \lfloor L_{f,s}(\overline{z}_{1_f})\rfloor_e \{\overline{A}_{f,s}(\overline{z}_f)\}_e, \tag{34}$$

$$\overline{b}_{f,s}(\overline{z}_f,\overline{z}_{1_f}) \approx \sum_{e=1}^{N_e} \lfloor L_{f,s}(\overline{z}_{1_f})\rfloor_e \{\overline{b}_{f,s}(\overline{z}_f)\}_e, \tag{35}$$

where $\lfloor L_{f,s}(\overline{z}_{1_f})\rfloor_e$ is a row vector of functions used to interpolate the fields and driving terms of the $e$th element from their nodal values as defined by the column vectors $\{\overline{A}_{f,s}(\overline{z}_f)\}_e$ and $\{\overline{b}_{f,s}(\overline{z}_f)\}_e$. The interpolation functions for the $e$th element are defined to be zero out with the range of $\overline{z}_{1_f}$ of the element.

In the electron frame of reference the slow mode is counterpropagating to the fast mode, and so the nodes are numbered in the opposite sense to those of the fast mode [Fig. 6(b)]. At each fast/slow node the driving terms $b_{f,s_n}$ are calculated from the sum over the number of electrons within a beat period, as illustrated in Fig. 6(c), consistent with the averaging of the wave equations over a beat period.

Consider the fields in the $e$th element only, and substitute Eqs. (34) and (35) into wave equations (17) and (18) and apply the ''Galerkin criterion'' [30], which assumes that with the approximation for fields (34), the left hand side of Eqs. (17) and (18) must be equal to the right hand side ''in some average sense.'' This average is taken by using the interpolation functions as weighting functions for the average. Premultiplying both sides of the wave equations by

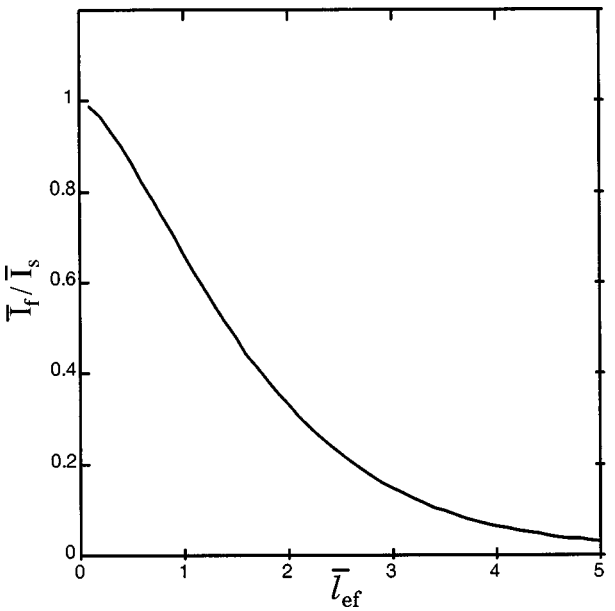


FIG. 5. The scaled intensity ratio $\bar{I}_f/\bar{I}_s$ as a function of scaled electron pulse length $\bar{l}_{e_f}$ for $\bar{z}_f=20$ and $\epsilon^3=4$. The intensity $\bar{I}_f$ is that of the higher frequency $\omega_f$ on exiting the electron pulse at its leading edge, $\bar{z}_{1_f}=\bar{l}_{e_f}$. The intensity $\bar{I}_s$ is that of the lower frequency $\omega_s$ on exiting the electron pulse at its trailing edge, $\bar{z}_{1_f}=0$.

$\{L_{f,s}(\bar{z}_{1_f})\}_e$, and integrating over a range $[-\infty,\infty]$ of $\bar{z}_{1_f}$, yields the elemental wave equations

$$[C_f]_e\left\{\frac{d\bar{A}_f}{d\bar{z}_f}\right\}_e=\{B_f\}_e-[K_f]_e\{\bar{A}_f\}_e, \tag{36}$$

$$[C_s]_e\left\{\frac{d\bar{A}_s}{d\bar{z}_f}\right\}_e=\{B_s\}_e+\epsilon^3[K_s]_e\{\bar{A}_s\}_e, \tag{37}$$

where the matrices $[C_f]_e$ and $[K_f]_e$ are given by

$$[C_{f,s}]_e=\int_{-\infty}^{\infty}\{L_{f,s}(\bar{z}_{1_f})\}_e\lfloor L_{f,s}(\bar{z}_{1_f})\rfloor_e d\bar{z}_{1_f}, \tag{38}$$

$$[K_{f,s}]_e=\int_{-\infty}^{\infty}\{L_{f,s}(\bar{z}_{1_f})\}_e\frac{d}{d\bar{z}_{1_f}}\lfloor L_{f,s}(\bar{z}_{1_f})\rfloor_e d\bar{z}_{1_f} \tag{39}$$

and

$$\{B_f\}_e=[C_f]_e\{\bar{b}_f\}_e, \tag{40}$$

$$\{B_s\}_e=\epsilon[C_s]_e\{\bar{b}_s\}_e. \tag{41}$$

The wave equations describing the evolution of the entire fields are constructed from the elemental wave equations describing the field evolution in each element. The coupling of one element to another arises from the common nodal field values of adjacent elements. The construction process and the application of the boundary conditions are clearly described in the literature [30].

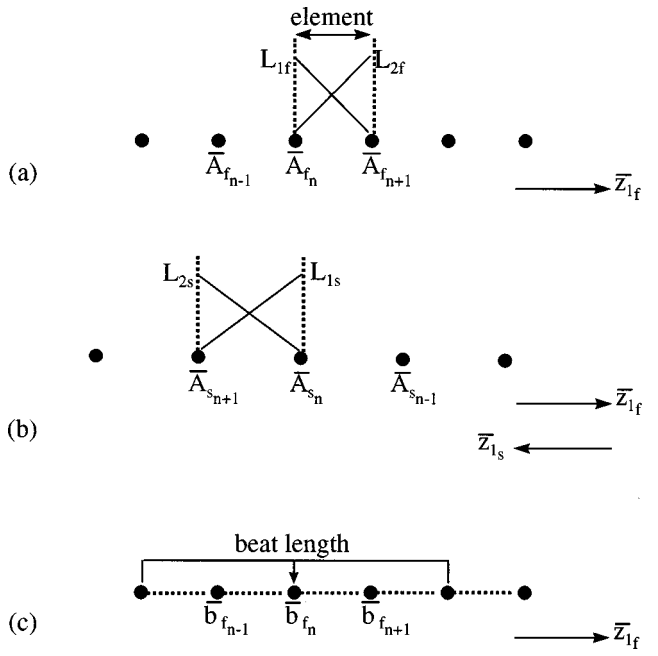


FIG. 6. (a) The interpolation functions $L_{1_f}$ and $L_{2_f}$ for the $n$th element of the fast mode. (b) The interpolation functions $L_{1_s}$ and $L_{2_s}$ for the $n$th element of the slow mode. (c) The nodal driving term $\bar{b}_{f_n}$ is found by averaging over the contributions of the electrons contained within a beat period.

Construction of the full wave equation from the elemental equations and application of the boundary conditions of the wave equation yields a system of ordinary differential equations in the scaled nodal field amplitudes $\bar{A}_{f,s_n}(\bar{z}_f)$:

$$[C_f]\left\{\frac{d\bar{A}_f(\bar{z}_f)}{d\bar{z}_f}\right\}=\{B_f\}-[K_f]\{\bar{A}_f\}, \tag{42}$$

$$[C_s]\left\{\frac{d\bar{A}_s(\bar{z}_f)}{d\bar{z}_f}\right\}=\{B_s\}+\epsilon^3[K_s]\{\bar{A}_s\}. \tag{43}$$

Here $\{B_{f,s}\}$ are the source terms due to the macroparticles, each field node being driven only by the macroparticles contained within the average over a beat centered at the node.

The set of ordinary differential equations (42) and (43) together with the particle equations (11)–(16) constitute a large system of ordinary differential equations which may be solved for the derivatives using standard sparse matrix solvers, and then integrated in $\bar{z}_f$ using, for example, a fourth order Runge-Kutta routine. The above model can be easily adapted to study one mode evolution when there is only one resonant frequency.

## V. ANALYSIS

In this section numerical solutions of the above model will be given for single mode and two mode interactions, and for long and short electron pulses. We begin by comparing the results of the linear analysis of Sec. III with numerical solutions from the model of Sec. IV. The analysis of the linear regime showed that the fast and slow modes decouple. In order to compare this analysis with the numerical model,

it is sufficient therefore to model two single mode interactions numerically with the appropriate fast and slow parameters.

A single mode interaction, either fast or slow, is then modeled numerically for both short and long electron pulses into the nonlinear regime. We demonstrate the superradiant scaling of the radiation emitted by a short electron pulse, termed ''weak superradiance'' in close analogy with that of FEL theory [26]. It is shown that the effect of increasing free energy depletion can destroy the superradiant nature of the emitted radiation. Furthermore, it is shown that the superradiant intensity emitted by a short electron pulse has an exponentially decaying dependence upon the depletion parameter $\mu$. This rate of decay becomes more pronounced on increasing the real length of the electron pulse. For long electron pulses the regime of ''strong superradiance'' is demonstrated. (Again this terminology is directly analogous to that of FEL theory.) The radiation emitted in the steady state region of a long pulse may be suppressed by choosing a value of the depletion parameter $\mu$ above the threshold value $\mu_{\rm th}$. In the slippage region of the pulse where superradiant emission may occur, and for larger values of $\mu$, we demonstrate that superradiant emission exists but is significantly reduced.

The full numerical model is then used to study the coupled interaction between fast and slow modes, and for short and long electron pulses. The linear theory of Sec. III suggested that a suppression of the slow mode may be possible by the choice of a suitably short electron pulse. Simulations demonstrate that this pulse suppression of the slow mode is enhanced when the interaction becomes nonlinear. It is shown that the higher frequency fast mode may in fact dominate the coupled interaction, yielding a true pulse suppression of the lower frequency slow mode. Furthermore, for short electron pulses weak superradiance is shown to exist for both slow and fast modes. On increasing the electron pulse length, and for sufficiently low free energy depletion, the slow mode becomes dominant with significantly reduced emission of the fast mode. In addition, strong superradiant emission of the slow mode is observable. Increasing the effects of free energy depletion by increasing $\mu$, steady state suppression of the slow mode only is possible using the $\mu$-suppression condition of Eq. (10). In this case the fast mode becomes dominant, and strong superradiance of this mode is observable. Increasing $\mu$ further also suppresses steady state fast mode growth, and significantly reduces strong superradiance.

### A. Comparison of numerical solutions with short pulse linear theory

Previous work has given both linear and numerical solutions for the two mode interaction in the steady state [16]. As with this previous work, the linear analysis for pulses of Sec. III showed that the fast and slow modes are decoupled. In order to compare our numerical solutions with this linear theory, we use a single mode model for the fast and slow modes. By single mode model, we mean that the electron/radiation interaction with either the fast or the slow mode may be artificially switched off in the numerical simulation.

The above linear theory of Fig. 5 shows that for short pulses the scaled intensities of the fast and slow modes are approximately equal, $\bar{I}_f \approx \bar{I}_s$. This is verified in Fig. 7, where we plot the scaled intensities for the two modes as functions of $\bar{z}_f$ as calculated by the linear theory, and directly compare with single mode numerical solutions for a short pulse of $\bar{l}_{e_f} = 0.26$. As with Fig. 5, the scaled intensities are those as they exit the electron pulse into vacuum, i.e., $\bar{I}_f(\bar{z}_{1_f} = \bar{l}_{e_f}, \bar{z}_f)$ and $\bar{I}_s(\bar{z}_{1_f} = 0, \bar{z}_f)$. The near equality of these fast and slow mode intensities can be seen from the superposition of the two linear theory plots, and the near superposition of the two numerical solutions in the linear regime $\bar{z}_f \lesssim 30$. The discrepancy between the linear and numerical solutions may be ascribed to the asymptotic form of the linear solution and the nonlinear effects in the numerical solution for larger values of $\bar{z}_f$. We stress here that the numerical solutions are for single mode uncoupled evolution, for the purposes of comparison with linear theory. It will be seen in Sec. V C that when coupling between the modes is included in the numerical model, this uncoupled linear theory quickly breaks down for significantly smaller values of $\bar{z}_f$.

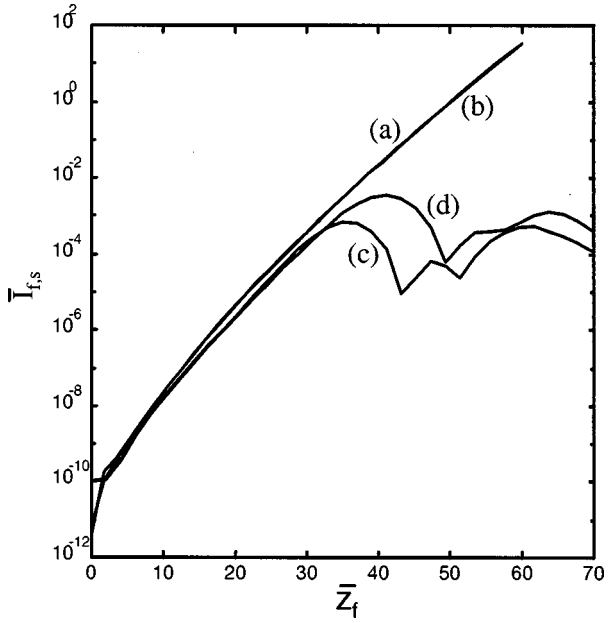


FIG. 7. A comparison of the linear [(a) fast; (b) slow] and numerical [(c) fast; (d) slow] scaled field intensities, for a single mode interaction: $\epsilon^3 = 4$, $\Omega = 2.0125$, $\bar{l}_{e_f} = 0.26$, $\rho_f = \mu_f = 0.01$, and $\bar{A}_{f_0} = \bar{A}_{s_0} = 10^{-5}$.

### B. Single mode superradiance

The emission from electron pulses is now investigated for a single mode interaction into the nonlinear regime. This is carried out using the single mode numerical model described in Sec. V A. We call the limit $\mu \ll 1$ the FEL limit as, for single mode interaction only, the scaled equations reduce to those describing the Compton FEL [13]. The similarities between the CRM and FEL theory extends to that of pulse interaction where, under specified conditions, radiation emitted may be superradiant. In superradiance the radiation intensity scales as the square of the number of emitters, $I \propto n_e^2$, where $n_e$ is the electron density. In the steady state

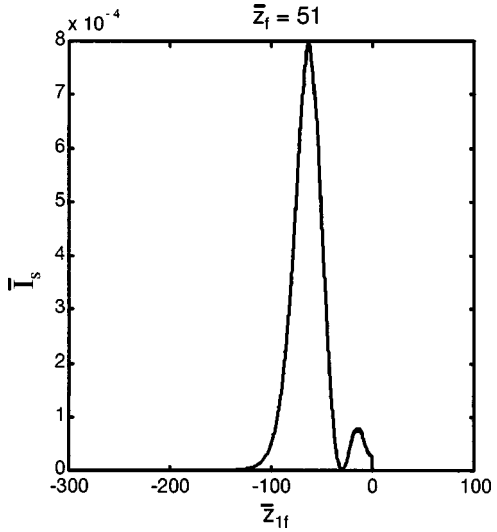


FIG. 8. Typical weak superradiant emission of the lower frequency slow mode by a short electron pulse and for single mode interaction: $\bar{l}_{e_f}=0.26$, $\rho_s=0.04$, $\mu_s=0.16$, $\bar{A}_{s_0}=10^{-5}$, $\bar{z}_f=51$, $\epsilon^3=4$, and $\Omega=2.0125$.

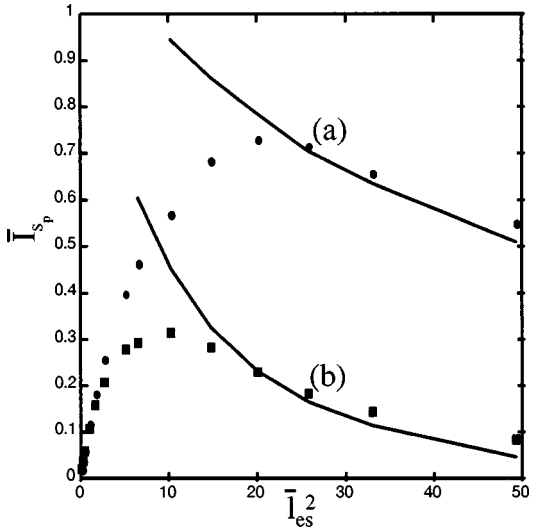


FIG. 9. Peak intensity as a function of $\bar{l}_{e_s}^2$ for two different values of $\nu_s$: (a) $\nu_s=0.25$ and (b) $\nu_s=0.1$. The solid lines give the results of the equivalent steady state numerical simulation.

regime, and in the FEL limit of the CRM, radiation intensities scale as $n_e^{4/3}$. It is easily shown that for the scaling used here, where $\rho \propto n_e^{1/3}$, superradiant emission occurs when the scaled intensity $\bar{I}=|\bar{A}|^2 \propto \rho^2$ and in the steady state FEL limit, $\bar{I}$ is $\rho$ independent. When free energy depletion effects become important, however, the steady state scaled intensity takes on the scaling $\bar{I} \propto 1/\mu$. For the case of a constant free energy parameter $\nu$ this scaling corresponds to a real intensity $I \propto n_e$.

#### *1. Short pulses*

As in the FEL, weak superradiance in a CRM is characterized by the emission of a pulse of radiation with a peak intensity significantly less than the saturation intensity of the steady state. Typical weak superradiant emission by a short electron pulse $\bar{l}_{e_f}=0.26$ ($\bar{l}_{e_s}=0.10$) is shown in Fig. 8. The case shown here is for an interaction at the lower frequency slow mode only, so that the group velocity of the radiation is less than that of the electrons and the radiation propagates from right to left in the figure, as $\bar{z}_f$ increases. Depending upon the value of $\mu_s$ the first peak of the scaled intensity, $\bar{I}_{s_p}$, here at $\bar{z}_{1_f} \approx -65$, may have a superradiant scaling.

This is demonstrated in Fig. 9, where we plot $\bar{I}_{s_p}$ as a function of the scaled length $\bar{l}_{e_s}^2$ for two different values of the free energy parameter $\nu_s$. The following two points should be noted with regard to the scaling. First, it has been assumed that the pulse length $l_e$ is a constant, so that $\bar{l}_{e_s} \propto \rho_s$ and superradiant scaling will occur when $\bar{I}_{s_p} \propto \bar{l}_{e_s}^2$. Second, from the definition of $\mu_s$ following Eq. (18), it is seen that if changes in $\rho_s$ are due to the electron current only, then the value of $\mu_s \propto \rho_s$. Hence, for a constant $\nu_s$, each graph of the figure has a value of $\mu_s$ which is in proportion to the value of $\bar{l}_{e_s}$. For the shorter electron pulses the linear dependence of $\bar{I}_{s_p}$ with $\bar{l}_{e_s}^2$ is clearly seen in Fig. 9(a), indicating superradiant emission. As the scaled electron pulse length increases so the superradiant proportionality between $\bar{I}_{s_p}$ and $\bar{l}_{e_s}^2$ breaks down. On increasing the scaled length further it is seen that $\bar{I}_{s_p}$ tends to that of the steady state value, indicated by the solid line which scales as $\bar{I}_{s_p} \propto 1/\mu_s \propto 1/\bar{l}_{e_s}$, corresponding to a real intensity scaling of $I_{s_p} \propto n_e$. On decreasing the value of $\nu_s$, in Fig. 9(b), it is seen that the increased effects of free energy depletion reduces the range in $\bar{l}_{e_s}$ over which superradiant scaling is observed. Decreasing the values of $\nu_s$ further, the suppression of superradiant emission is observed for $\bar{l}_{e_s} \lesssim 1$.

The scaling of the peak intensity $\bar{I}_{s_p}$ as a function of the depletion parameter $\mu_s$ is now investigated for three different short-scaled electron pulse lengths, $\bar{l}_{e_s}$. The value of $\rho_s$ for each graph is a constant, so that the variation in $\mu_s$ results from a variation in the free energy parameter $\nu_s$ only. It is seen from Fig. 10 that there is a near exponentially decreasing dependence of the intensity with depletion parameter $\mu_s$ and that the longer pulses have a larger saturation intensity than the shorter pulses. These larger intensities result in the electrons becoming energy depleted more readily, and the rate of decrease with $\mu_s$ is more pronounced.

#### *2. Long pulses and μ suppression*

In addition to weak superradiance, a regime called strong superradiance may also exist in the slippage regions of long electron pulses ($\bar{l}_e \gg 1$), and can give rise to radiation spikes with peak intensities significantly greater than that of the steady state. Previous descriptions of strong superradiance have been given for the FEL, where it has been described in terms of the weak superradiance emitted by the slippage region of the electron pulse which has been amplified on propagating further through the electron pulse [24–26]. Essentially the same mechanism may occur in the CRM with the added feature of free energy depletion. A typical strong

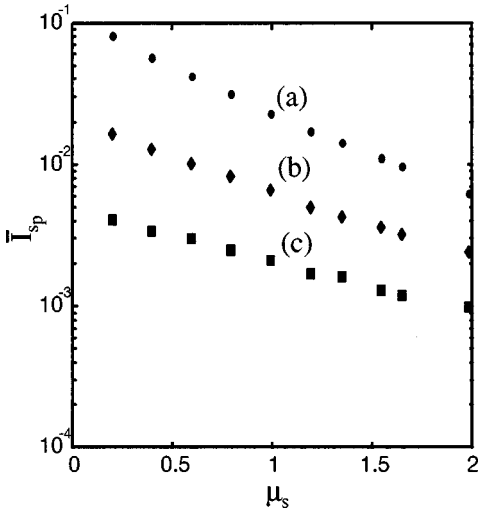


FIG. 10. Peak intensity as a function of $\mu_s$ for three different short pulse lengths: (a) $\rho_s=0.08$; $\bar{l}_{e_f}=3$; (b) $\rho_s=0.04$, $\bar{l}_{e_f}=1$; (c) $\rho_s=0.02$, $\bar{l}_{e_f}=0.5$, $\epsilon^3=4$, and $\Omega=2.0125$.

superradiant emission is demonstrated in Fig. 11. As with the short pulse example, interaction with the slow mode is considered. The slippage region is now at the front of the electron pulse, as seen in Fig. 3, and as with the short pulse case of above, the radiation propagates from right to left as the interaction progresses. The radiation in this figure may be broken down into three regions which are, from left to right in the figure, the vacuum region, where the radiation has propagated outside of the electron pulse into vacuum; the steady state region, which has an intensity which is $\bar{z}_1$ independent; and the slippage region where strong superradiance may be observed. On propagating into vacuum the radiation from the steady state no longer interacts and merely propagates. Hence the vacuum radiation describes a ''history'' of the steady state evolution, and the usual steady state intensity evolution, of exponential growth followed by saturation and oscillation, is clearly seen. In the slippage region the strong superradiant spiking is observed with an intensity significantly greater than that of the steady state saturation value.

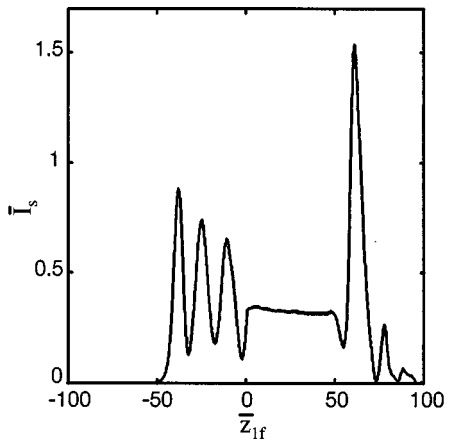


FIG. 11. Typical strong superradiant emission from a long electron pulse: $\bar{l}_{e_f}=100$, $\rho_s=0.04$, $\mu_s=0.16$, $\bar{A}_{s_0}=10^{-5}$, $\bar{z}_f=15$, $\epsilon^3=4$, and $\Omega=2.0125$.

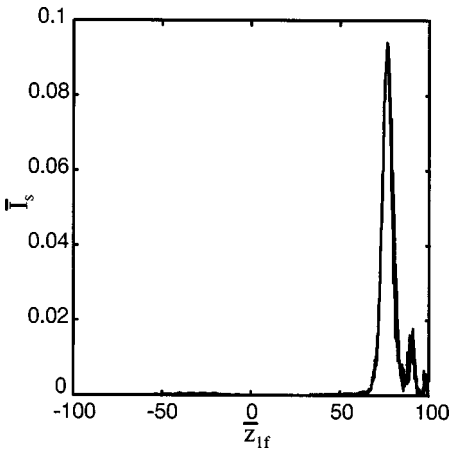


FIG. 12. Suppression of the steady state evolution for $\mu>\mu_{\rm th}$: $\bar{l}_{e_f}=100$, $\rho_s=0.04$, $\mu_s=1.03$, $\bar{A}_{s_0}=10^{-5}$, $\bar{z}_f=15$, $\epsilon^3=4$, and $\Omega=2.0125$.

For the same long pulse we now set the depletion parameter above the threshold value $\mu_s=1.03>\mu_{\rm th}$. In this case no exponential increase in the steady state intensity is possible, as is seen from Fig. 12. Again, as with the short pulse case, this threshold does not apply to the slippage region where a significant evolution of the radiation intensity is observed. The superradiant evolution of the pulse is seen to be significantly reduced from that of Fig. 11. This may be attributed not only to the increase in the effect of free energy depletion, as $\mu_s$ has been increased by a factor of 6.5, but also to the increase in the region of nonexponential interaction shown in Fig. 4 and defined by Eq. (29). The region of no exponential instability, in the nonsuppressed case of Fig. 11, is $40.64<\bar{z}_{1_f}<40.69$, and for the suppressed case of Fig. 12 is extended to $40.64<\bar{z}_{1_f}<54.53$. Not only is there no exponential instability in this region of the pulse, but the existing superradiant pulse is unable to propagate into this region. This is clearly demonstrated by comparing the positions of the peaks of the superradiant pulses between Figs. 11 and 12.

### C. Coupled mode superradiance

The full numerical model is now used to investigate the coupled evolution of both the fast and slow modes with the electron pulse. These results therefore supersede those of the single mode analysis of previous sections. The electron pulse now emits two distinct radiation pulses: a slow mode pulse described in Sec. V B 1 that propagates in the direction of negative $\bar{z}_{1_f}$, and a fast mode pulse that propagates in the direction of positive $\bar{z}_{1_f}$. An example of a full numerical solution to the coupled evolution equations demonstrating such emission is shown in Fig. 13. The peak of the slow mode emission is at $\bar{z}_{1_f}\approx-18$, and that of the fast mode is at $\bar{z}_{1_f}\approx5$.

#### *1. Short pulses and pulse suppression of the slow mode*

The linear theory of Sec. III suggested that it may be possible to suppress the growth of the slow mode by choos-

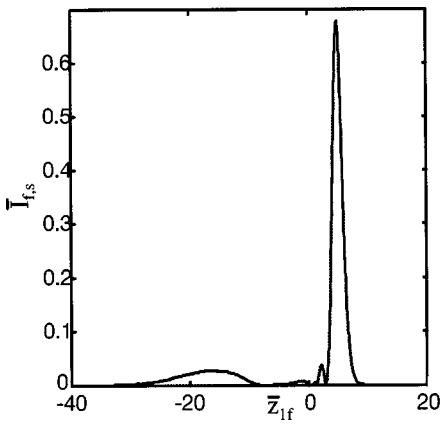


FIG. 13. Coupled interaction showing both slow and fast mode emission: $\epsilon^3=4$, $\Omega=2.0125$, $\bar{l}_{e_f}=2.61$, $\rho_f=0.08$, $\mu_f=0.08$, $\bar{A}_{f0}=0$, $\bar{A}_{s0}=10^{-5}$, and $\bar{z}_f=20$.

ing an electron pulse that is sufficiently short. Furthermore, the radiation emitted may also exhibit superradiant scaling. A full numerical solution to the coupled evolution equations is shown in Fig. 14. An identical set of parameters as those used to obtain the uncoupled results of Fig. 7 were used, with the exception that in the coupled mode evolution of Fig. 14 the initial field for the fast mode was set to zero ($\bar{A}_{f_0}=0$). The results demonstrate that not only does the peak scaled intensity of the fast mode approach that of the slow, as suggested by the linear theory, but that in the nonlinear regime the fast mode actually dominates the interaction, the fast mode scaled peak intensity being greater than one order of magnitude above that of the slow mode. This fast mode domination of the interaction may be understood in terms of two distinct mechanisms. The first is that of pulse suppression, which results from the shorter scaled length of the electron pulse in the case of the slow mode as described above. The second is the ''enhanced emission'' of the fast mode due

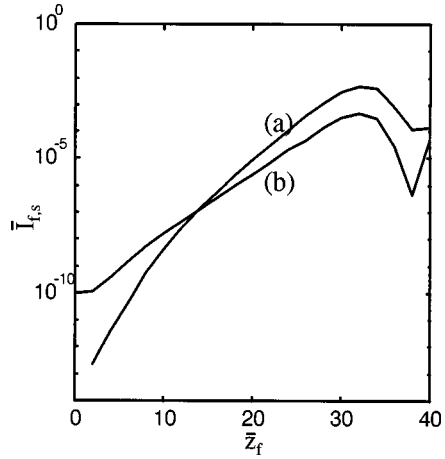


FIG. 14. Scaled intensities (a) $\bar{I}_f$ and (b) $\bar{I}_s$, for the coupled numerical model. The intensity $\bar{I}_f$ is that of the higher frequency $\omega_f$ on exiting the electron pulse at its leading edge, $\bar{z}_{1_f}=\bar{l}_{e_f}$. The intensity $\bar{I}_s$ is that of the lower frequency $\omega_s$ on exiting the electron pulse at its trailing edge, $\bar{z}_{1_f}=0$. Here $\epsilon^3=4$, $\Omega=2.0125$, $\bar{l}_{e_f}=0.26$, $\rho_f=0.1$, $\mu_f=0.1$, $\bar{A}_{f0}=0$, and $\bar{A}_{s0}=10^{-5}$.

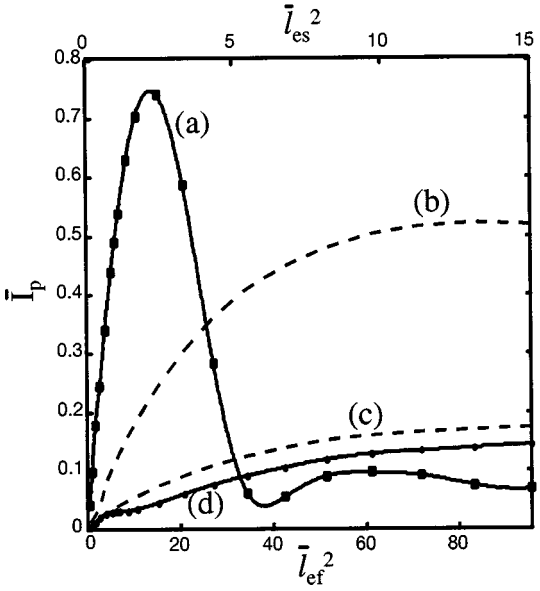


FIG. 15. Demonstration of pulse suppression showing the peak scaled intensities of the fast and slow modes ($I_{f_p}$ and $I_{s_p}$ respectively) as functions of $\bar{l}_{e_f}^2$ (and $\bar{l}_{e_s}^2$ on the upper axis): $\epsilon^3=4$, $\Omega=2.0125$, $\nu_f=1$, $\nu_s=0.25$, $\bar{A}_{f0}=10^{-8}$ (uncoupled), $\bar{A}_{f0}=0$ (coupled), and $\bar{A}_{s0}=10^{-5}$. (a) Coupled fast mode. (b) Uncoupled fast mode. (c) Uncoupled slow mode. (d) Coupled slow mode.

to the electron phase bunching of the slow mode interaction. This nonlinear parametric coupling is also observed in the steady state evolution, where no pulse effects are present [16], and accounts for the rapid growth of the fast mode from zero initial intensity in Fig. 14. We note that the ability of the fast mode to dominate the interaction is sensitive to the initial values of the magnitudes of both the fast and slow fields $|\bar{A}_{f_0}|$ and $|\bar{A}_{s_0}|$. If the latter is too large, it has been observed that the fast mode may not attain dominance before the slow mode reaches saturation. This sensitivity to initial values will be investigated further in future work.

In Fig. 15, the peak scaled intensities of the coupled fast and slow modes, $\bar{I}_{p_f}$ and $\bar{I}_{p_s}$, respectively, are plotted as functions of the square of the scaled electron pulse length $\bar{l}_{e_f}^2$. The square of the scaled electron pulse length for the slow mode $\bar{l}_{e_s}^2$ is shown on the upper axis, the two being related via $\bar{l}_{e_f}=\epsilon^2\bar{l}_{e_s}$. The solid lines show the result of a full coupled numerical solution, whereas the dashed lines show the corresponding single mode evolutions of the fast and slow modes. Note that for the single fast mode evolution the initial field amplitude is nonzero ($\bar{A}_{f_0}=10^{-8}$), whereas that for the coupled mode is zero, the initial fast mode field growth occurring due to the enhanced emission described above. The results of Fig. 15 are the two mode equivalent of Fig. 9 but for only one value of free energy parameter $\nu_f$. The same scaling applies: superradiant scaling is demonstrated when the peak intensity $\bar{I}_{p_{f,s}}$ of an emitted pulse has a linear dependence with $\bar{l}_{e_f}^2$.

For the longer pulse lengths of the figure, $\bar{l}_{e_f}^2 \gtrsim 80$, it is seen that the slow mode dominates the coupled interaction so

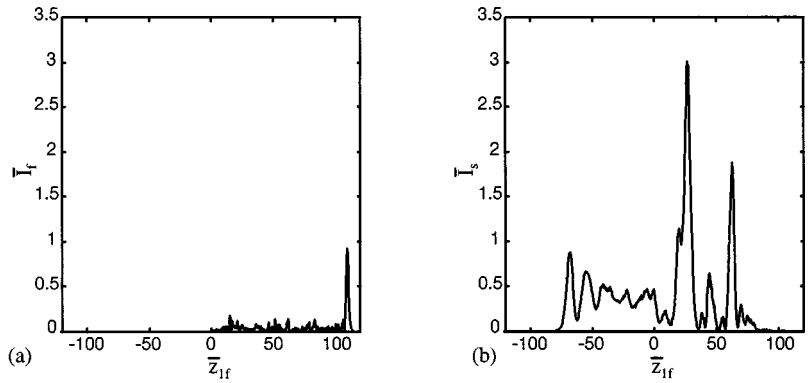


FIG. 16. Intensities of the coupled interaction for a long electron pulse. (a) Fast mode. (b) Slow mode. $\epsilon^3=4$, $\Omega=2.0125$, $\bar{l}_{e_f}=100$, $\rho_f=0.1$, $\mu_f=0.1$, $\bar{A}_{f0}=10^{-5}$, $\bar{A}_{s0}=10^{-5}$, and $\bar{z}_f=32$.

that the fast mode intensities are significantly less than those for evolution of the fast mode alone. This is consistent with previous results for the coupled steady state interaction [16] to which the pulsed interaction tends in the limit of very long pulses $\bar{l}_{e_{f,s}} \gg 1$.

For the shorter pulse interactions $\bar{l}^2_{e_f} \lesssim 30$ ($\bar{l}^2_{e_s} \lesssim 5$), the electron pulse is long with respect to the fast mode but short with respect to the slow mode. This, and the enhanced emission of the fast mode, allows the latter to dominate the interaction significantly. Using the relation (33) and the parameters of this interaction ($\epsilon^3=4$ and $\Omega=2.0125$), then for a scaled electron pulse length $\bar{l}_{e_f} \approx 4$ the unscaled intensity of the fast mode is approximately 40 times greater than that of the slow mode. Furthermore, the intensities of the fast mode interaction in this regime are actually greater than those attained for the single mode evolution of the fast mode. We call this mechanism of suppression of the lower frequency slow mode pulse suppression.

For pulse lengths $0<\bar{l}^2_{e_f} \lesssim 4$ ($0<\bar{l}^2_{e_s} \lesssim 1$), and for the coupled interaction, superradiant scaling of both the fast and slow modes is observed. Note that the slow mode coupled results are almost coincident with those of the single slow mode in this region. This has similarities with the evolution of superradiant pulses in atomic systems, where for sufficiently short systems, the counterpropagating radiation pulses evolve independently [31].

#### *2. Long pulses and μ suppression of the slow mode*

Long electron pulses give rise to steady state evolution within the main body of the pulse and possible strong superradiant evolution in the slippage regions, as was discussed in Sec. V B 2 for the single mode interaction. Inspection of Fig. 3, however, shows that for a coupled interaction it is not possible for the steady state radiation to propagate into vacuum without first propagating through a slippage region of the electron pulse. Hence the radiation propagating in vacuum does not necessarily describe the history of the coupled steady state evolution, as occurred for the single mode as described in Sec. V B 2.

A typical plot of the intensities of the fast and slow mode coupled interaction for a long electron pulse $\bar{l}_{e_f}=100$ is shown in Fig. 16. The fast mode radiation [Fig. 16(a)] has a peak in the intensity at $\bar{z}_{1_f} \approx 110$ which is higher than expected for the steady state coupled interaction. This may be explained by the emission process in the slow mode slippage region, including enhanced emission of the fast mode. This region initially evolves in a similar way to that of a shorter electron pulse as described in Sec. V C 1, and we observe a fast mode pulse which is of similar intensity to the maximum of Fig. 15(a). The analysis of Sec. V C 1 discussed the sensitivity of this emission of the fast mode to the initial fields $|\bar{A}_{f_0}|$ and $|\bar{A}_{s_0}|$. As there, if the latter field is too large, it has been observed that the fast mode pulse of Fig. 16(a) may not become dominant before the slow mode reaches saturation.

In the fast mode slippage region there is no enhanced emission of the slow mode, and this region evolves similarly to that of the coupled steady state, which dominates any fast mode superradiant emission. Hence as with the single mode evolution, the slow mode radiation propagating into vacuum describes the history of its evolution. Figure 16(b) shows strong superradiant emission of the slow mode at $\bar{z}_{1_f}=25$, with a peak intensity greater than that of the steady state saturation value. It can be seen by comparing Figs. 16(a) and 16(b) that, except for the fast mode emission from the slow mode slippage region, the slow mode clearly dominates the interaction and the fast mode does not exhibit any strong superradiant behavior.

For a coupled interaction, it is possible to use the $\mu$-suppression condition (10) to suppress the exponential growth of the slow mode. An identical set of parameters to those of Fig. 16 are used, with the exception that the depletion parameter is set to $\mu_f=0.65$. It is observed in Figs. 17(a) and 17(b) that the slow mode is suppressed and the fast mode is now dominant. Again, as with the one mode case, the $\mu$ suppression does not apply in the slow mode slippage region where superradiant evolution of the slow mode is observed, but is significantly reduced. As with suppression of the single slow mode of Sec. V B 2, the reduced slow mode emission may be attributed not only to the increase in the depletion parameter, but also to the expansion of the region of nonexponential interaction defined by Eq. (29). The formation of the strong superradiant spike of the fast mode is seen at $\bar{z}_{1_f}=10$. The spike has a peak intensity greater than that of the steady state saturation value, and is amplified as it propagates through the electron pulse in the direction of positive $\bar{z}_{1_f}$.

## VI. CONCLUSIONS

We have presented a detailed analytical and numerical investigation of CRM's operating in the pulsed amplifier re-

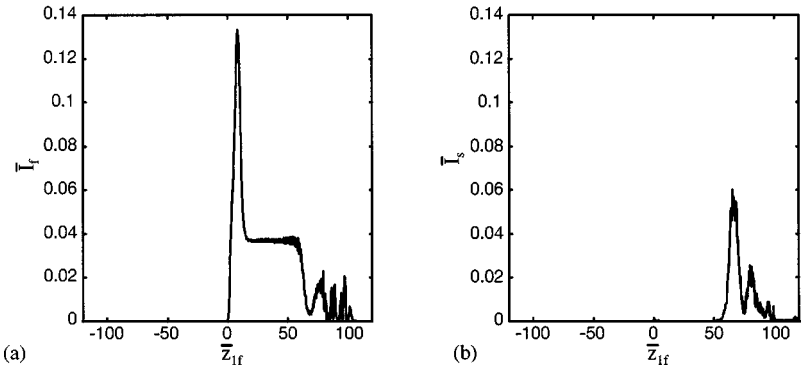


FIG. 17. Demonstration of slow mode $\mu$ suppression within the steady state region of the long pulse. (a) Fast mode. (b) Slow mode. $\epsilon^3=4$, $\Omega=2.0125$, $\bar{l}_{e_f}=100$, $\rho_f=0.1$, $\mu_f=0.65$, $\bar{A}_{f0}=10^{-5}$, $\bar{A}_{s0}=10^{-5}$, and $\bar{z}_f=32$.

gime which has yielded significant results. Superradiant emission has been demonstrated, and it was shown that, in general, the coupled interaction between both resonant frequencies must be taken into account. Both an analytic linear and a nonlinear numerical analysis of the equations of evolution were given, the former suggesting two possible methods of suppressing the lower frequency interaction which, in the steady state, usually dominates the interaction. A numerical solution of the evolution equations showed that these two methods, $\mu$ suppression and pulse suppression, extend into the nonlinear regime of evolution. Pulse suppression may occur for short electron pulse lengths. Nonlinear evolution enhances the effects of pulse suppression predicted by the linear analysis, so that the higher frequency interaction dominates. Another feature of the interaction with short electron pulses is weak superradiant evolution at both of the resonant frequencies. For long pulses a strong superradiant evolution of the radiation is observed in the simulations.

The model presented here has suggested regimes of operation of the CRM with significant practical potential, i.e., the generation of short pulses of high-frequency, high-power microwave radiation. Further work is now required to extend the model to include effects such as energy spread and space-charge in the electron beam, and waveguide dispersion.

## ACKNOWLEDGMENTS

The authors would like to thank the EPSRC for support of P.A. and B.W.J.McN., and the Royal Society of Edinburgh for support of G.R.M.R.

[1] P. Sprangle and A. T. Drobot, IEEE Trans. Microwave Theory Tech. **25**, 528 (1977).
[2] V. L. Bratman and G. G. Denisov, Int. J. Electron. **72**, 969 (1992).
[3] G. Bekefi, A. DiRienzo, C. Leibovitch, and B. G. Danly, Appl. Phys. Lett. **54**, 1302 (1989).
[4] S. H. Gold, D. A. Kirkpatrick, A. W. Fliflet, R. B. McCowan, A. K. Kinkead, D. L. Hardesty, and M. Sucy, J. Appl. Phys. **69**, 6696 (1991).
[5] A. DiRienzo, G. Bekefi, C. Chen, and J. S. Wurtele, Phys. Fluids B **3**, 1755 (1991).
[6] V. L. Bratman, N. S. Ginzburg, G. S. Nusinovich, M. I. Petelin, and P. S. Strelkov, Int. J. Electron. **51**, 541 (1981).
[7] A. W. Fliflet, M. E. Read, K. R. Chu, and R. Seeley, Int. J. Electron. **53**, 505 (1982).
[8] A. K. Ganguly and S. Ahn, Int. J. Electron. **53**, 41 (1982).
[9] A. W. Fliflet, Int. J. Electron. **61**, 1049 (1986).
[10] K. D. Pendergast, B. G. Danly, R. J. Tempkin, and J. S. Wurtele, IEEE Trans. Plasma Sci. **16**, 122 (1988).
[11] K. R. Chu and A. T. Lin, IEEE Trans. Plasma Sci. **16**, 90 (1988).
[12] C. Chen and J. S. Wurtele, J. Phys. D **3**, 2133 (1991).
[13] B. W. J. McNeil, G. R. M. Robb, and A. D. R. Phelps, J. Phys. D **27**, 1092 (1994).
[14] G. R. M. Robb, Phys. Rev. E **50**, R3345 (1994).
[15] B. W. J. McNeil, G. R. M. Robb, and A. D. R. Phelps, J. Phys. D **30**, 1688 (1997).
[16] P. Aitken, B. W. J. McNeil, G. R. M. Robb, and A. D. R. Phelps, J. Phys. D **30**, 2482 (1997).
[17] P. Michelato, Nucl. Instrum. Methods Phys. Res. A **393**, 455 (1997), and references therein.
[18] G. A. Mesyats, V. G. Shpak, M. I. Yalandin, and S. A. Shunailov, in *Proceedings of the 8th International Pulsed Power Conference, San Diego, California, 1991* (IEEE, New York, 1991), p. 73.
[19] M. Garven, A. D. R. Phelps, S. N. Spark, D. F. Howell, and N. Cade, Vacuum **45** (1994).
[20] M. Garven, S. N. Spark, A. W. Cross, S. J. Cooke, and A. D. R. Phelps, Phys. Rev. Lett. **77**, 2320 (1996).
[21] N. S. Ginzburg, I. V. Zotova, A. S. Sergeev, I. V. Konoplev, A. D. R. Phelps, A. W. Cross, S. J. Cooke, V. G. Shpak, M. I. Yalandin, S. A. Shunailov, and M. R. Ulmaskulov, Phys. Rev. Lett. **78**, 2365 (1997).
[22] N. S. Ginzburg and A. S. Sergeev, Opt. Commun. **91**, 140 (1992).
[23] G. R. M. Robb, B. W. J. McNeil, and A. D. R. Phelps, in *Proceedings of the 19th International Conference on Infrared and Millimeter Waves, Sendai, Japan* (JSAP Report No. AP941228), edited by K. Sakai and T. Yoneyama (JSAP, Tokyo, 1994), p. 155.
[24] R. Bonifacio and B. W. J. McNeil, Nucl. Instrum. Methods Phys. Res. A **272**, 280 (1988).
[25] R. Bonifacio, C. Maroli, and N. Piovella, Opt. Commun. **68**, 369 (1988).

[26] R. Bonifacio, B. W. J. McNeil, and P. Pierini, Phys. Rev. A **40**, 4467 (1989).
[27] J. R. Pierce, *Travelling-Wave Tubes* (Van Nostrand, New York, 1950).
[28] P. Aitken, B. W. J. McNeil, G. R. M. Robb, and A. D. R. Phelps, Nucl. Instrum. Methods Phys. Res. A **407**, 136 (1998).
[29] R. Bonifacio, F. Casagrande, and L. De Salvo Souza, Opt. Commun. **58**, 259 (1986), and references therein.
[30] E. A. Huebner, E. A. Thornton, and T. G. Byrom, *The Finite Element Method for Engineers* (Wiley, New York, 1995).
[31] J. C. MacGillivray and M. S. Feld, Phys. Rev. A **14**, 1169 (1976).